International Journal of Fatigue 136 (2020) 105598

Contents lists available at ScienceDirect

International Journal of Fatigue

journal homepage: www.elsevier.com/locate/ijfatigue

Fatigue behavior and microstructural evolution of additively manufactured Inconel 718 under cyclic loading at elevated temperature

P.D. Nezhadfar[a,b], Alexander S. Johnson[c], Nima Shamsaei[a,b,*]

[a] Department of Mechanical Engineering, Auburn University, Auburn, AL 36849, USA
[b] National Center for Additive Manufacturing Excellence (NCAME), Auburn University, Auburn, AL 36849, USA
[c] TriVector Services Incorporated, Huntsville, AL 35801, USA

ARTICLE INFO

Keywords:
Laser beam directed energy deposition (LB-DED)
Inconel 718
Fatigue
Elevated temperature
Microstructure

ABSTRACT

This study investigates the fatigue behavior of Inconel 718 (IN718) fabricated through laser beam directed energy deposition (LB-DED) process. Fully-reversed ($R_\varepsilon = -1$) strain-controlled fatigue tests are conducted on LB-DED IN718 specimens at 650 °C and the results are compared with those of LB-DED IN718 specimens tested at room temperature as well as the ones obtained from wrought counterparts at both room temperature and 650 °C. The microstructure is characterized after fabrication, heat treatment, and fatigue tests at elevated temperature. Microstructure characterizations reveal that as-built LB-DED IN718 has a dendritic structure. The heat treatment applied could not eliminate the dendritic structure, and needle-like δ phases are formed on the grain boundaries. The comparison of LB-DED and wrought fatigue results show that the LB-DED IN718 possesses slightly lower fatigue resistance at room temperature, while exhibits a comparable fatigue strength at elevated temperature. In the low cycle regime, the fatigue resistance of LB-DED IN718 tested at elevated temperature is somewhat inferior to the ones tested at room temperature, which can be explained by the formation and growth of brittle needle-like δ and Laves phases on the grain boundaries during fatigue testing at elevated temperature and their effects on increasing the fatigue crack growth rate. In the high cycle regime, however, LB-DED IN718 specimens tested at elevated temperature had somewhat similar fatigue lives to the ones tested at room temperature. This may be partially explained by the surface oxidation during fatigue testing at elevated temperature, which can retard the microstructurally short cracks to grow.

1. Introduction

Nickle-based superalloys are widely used material systems in the aerospace industry due to their high temperature strength, as well as high creep and corrosion resistance [1]. Inconel 718 (IN718) is one of the most commonly used nickel-iron based superalloys, which has a face-centered cubic (FCC) microstructure and can be strengthened by a means of precipitation hardening mechanism. IN718 contains a high amount of Nb which strengthens the material by the formation of coherent γ″ (Ni_3Nb) and γ′ (Ni_3Al) precipitates in the γ matrix. On the other hand, the brittle Laves $(Ni,Fe,Cr)_2(Nb,Mo,Ti)$ phase is formed on the grain boundaries due to the low diffusion rate of Nb to the matrix. The γ″ is a metastable phase, which can transform to δ (Ni_3Nb) phase [2]. It has been reported that the δ (Ni_3Nb) phase is not associated with the strengthening of the material and while it reduces the fracture toughness, a high amount of δ phase can assist with the creep resistance at elevated temperature. [3].

Attaining the appropriate microstructure for IN718 to achieve the required properties for specific applications is associated with the primary manufacturing technique as well as the post process heat treatment. It is worth noting that IN718 possesses good weldability due to the sluggish precipitation kinetics [4]. On the contrary, this material suffers from poor machinability due to its high hardness and wear resistance [5]. Considering the favorable weldability and high cost of machining, IN718 is an attractive alloy for additive manufacturing (AM). Laser beam directed energy deposition (LB-DED) is one of the AM techniques in which a laser beam is used to create a melt pool for the powder to be sprayed in and build tracks after tracks, and layers after layers to create a 3D object from bottom to top [6].

Due to the rapid melting and solidification during AM process, AM parts experience intricate thermal history, which influences their microstructure and mechanical properties [7,8]. There are many reports on the microstructure heterogeneity and anisotropic mechanical properties of various AM materials, specifically in as-fabricated condition

* Corresponding author at: Department of Mechanical Engineering, Auburn University, Auburn, AL 36849, USA.
E-mail address: shamsaei@auburn.edu (N. Shamsaei).

https://doi.org/10.1016/j.ijfatigue.2020.105598
Received 18 January 2020; Received in revised form 12 March 2020; Accepted 13 March 2020
Available online 14 March 2020

Nomenclature

b	Fatigue strength exponent
E	Modulus of elasticity
N_f, $2N_f$	Cycles to failure, Reversals to failure
R_ε	Ratio of minimum strain to maximum strain
γ'	Matrix phase in the microstructure of IN718
σ_f'	Fatigue strength coefficient
σ_y	Yield strength
σ_u	Ultimate strength
ε_a	Total strain amplitude
ε_y	Yield strain
$\frac{\Delta\varepsilon_p}{2}$	Plastic strain amplitude
$\frac{\Delta\varepsilon_e}{2}$	Elastic strain amplitude

Abbreviations

AM	Additive manufacturing/Additively manufactured
BSD	Back scattered detector
DSA	Dynamic strain aging
EBM	Electron beam melting
FCC	Face-centered cubic
HIP	Hot isostatic pressing
Inconel 718	IN718
LB-DED	Laser beam directed energy deposition
LB-PBF	Laser beam powder bed fusion
RT	Room temperature
SEM	Scanning electron microscope/microscopy
STA	Solution treatment and aging
UTS	Ultimate tensile strength
YS	Yield strength

[6,9–12]. While there are several studies in the literature dealing with the microstructure and tensile behavior of AM IN718, there are only limited works available on the fatigue behavior of this material.

Lambarri et al. [13] compared the microstructure of the LB-DED IN718 with that of the wrought counterpart in the as-deposited, solution treated, and aged conditions. Unlike the wrought IN718, they observed dendritic microstructure for as-deposited LB-DED IN718 due to the very high cooling rate experienced in the LB-DED process. Although the dendritic structure remained in the microstructure of LB-DED IN718 after heat treatment, similar precipitates in both LB-DED and wrought IN718 were found.

Blackwell [14] investigated the effect of heat treatment and hot isostatic pressing (HIP) on the microstructure and tensile behavior of LB-DED IN718. Some of the specimens were solution annealed at 980 °C for 1 h and air cooled, followed by a double age procedure (i.e. 720 °C for 8 h, then furnace cooling followed by 620 °C for 8 h, then air cooling), and some of the specimens were HIPed at 1160 °C for 3 h with a pressure of 100 MPa prior to the double age heat treatment. The as-deposited LB-DED material had lower yield and ultimate tensile strength, and slightly higher ductility than the wrought counterpart. Performing the heat treatment, while significantly decreased the ductility (a 65% reduction), improved the strength close to the wrought material. HIPing were found to be effective to increase the ductility of the LB-DED material up to half of the one for the wrought counterpart.

Zhai et al. [15] studied the effect of process parameters and post thermal treatments on the tensile properties of LB-DED IN718. They observed fine dendritic microstructure with negligible Nb segregation as well as fine Laves phases after fabrication. They reported that using higher laser powers during fabrication can slightly increase the yield strength and ductility of the non-heat treated material as compared to the specimens fabricated using lower laser powers. Regarding the post thermal treatment, short aging procedure was observed to increase the yield strength of both the high- and low-laser power fabricated materials by 76% and 96%, while decreased the ductility by 61% and 58%, respectively.

Johnson et al. [16] investigated the fatigue behavior of LB-DED IN718 specimens at room temperature and compared the results to those obtained from wrought counterparts. The specimens (i.e. wrought [17] and LB-DED IN718) were solution annealed at 940 °C for 2 h, air cooled, and then aged at 718 °C for 8 h, cooled to 621 °C with the rate of 50 °C/h and kept at this temperature for 8 h followed by air cooling. They reported that LB-DED IN718 in machined surface condition had lower fatigue strength as compared to the wrought material due to the presence of pores or inclusions in the LB-DED IN718 specimens. They also reported a transgranular crack growth mechanism for LB-DED IN718 at room temperature.

Komarasamy et al. [18] examined the effect of powder atomization media as well as the microstructure on the fatigue and impact toughness properties of laser beam powder bed fused (LB-PBF) IN718 undergone AMS 2772 heat treatment procedure (i.e. solution annealing at 954 °C for 1 h, then air cooling, followed by aging at 718 °C for 8 h, then furnace cooling). Fatigue results exhibited an independency to the powder atomization media. They stated that elimination of the δ phases formed on the grain boundaries after heat treatment was effective in improving the fatigue strength of LB-DED IN718 as compared to that of the wrought material. In addition, LB-PBF IN718 possessed comparable impact toughness to the wrought counterpart due to the presence of δ phase.

Wan et al. [19] reported the enhancement in fatigue performance of LB-PBF IN718 after heat treatment. They performed three different heat treatment procedures; (1) solutionizing (980 °C for 1 h then air cooling) followed by aging (760 °C for 10 h followed by furnace cooling at the rate of 55 °C/h to 650 °C, and aging at this temperature for 8 h followed by air cooling), (2) homogenizing (1065 °C for 1 h then air cooling) followed by the same aging process, and (3) homogenizing, then solutionizing followed by the same aging process. All the heat treatment procedures improved the fatigue performance of the material as compared to the non-heat treated condition due to the elimination of Laves phases and the precipitation of γ′ and γ″ in the microstructure. The specimens undergone the heat treatment (2) even exhibited the best fatigue performance as compared to the other heat treatments. This was associated with the formation of needle-like δ phase, which attenuated the detrimental effects of pores on the fatigue strength of the LB-PBF IN718.

Balachandramurthi et al. [20] studied the microstructure related room temperature fracture mechanism through fatigue testing (R_ε = 0.1) on IN718 fabricated by electron beam melting (EBM) and LB-PBF techniques. They investigated the grain growth after the HIP process followed by solution treatment and the aging process (STA). It was shown that the δ phase formed on the grain boundaries after STA; however, there was no δ phase formed in HIP + STA condition. The fracture mechanisms were found to be influenced by the grain size. In case of the larger grains as a result of HIP + STA condition, the cracks propagated by a single shear mechanism, whereas cracks would grow by duplex slip mechanism in the finer grains, forming the striation marks.

While IN718 is often used in elevated temperature applications, most of the literature on the fatigue characterization of AM IN718 are related to the room temperature behavior. In a study, Sui et al. [21] investigated the effect of Laves phase on the high cycle fatigue properties of LB-DED IN718 at elevated temperature. They observed that the Laves phases maintain their morphology at lower stress amplitude levels and force the cracks to detour them and propagate in the γ matrix. On the contrary, at higher stress amplitude levels, Laves phases were

found to break and accelerate the crack growth process.

Despite the limited research on the fatigue behavior of LB-DED IN718 at elevated temperatures, extensive work has been done on the elevated temperature fatigue behavior of wrought IN718 [17,22–25]. Kawagoishi et al. [23] investigated the rotary bending fatigue behavior of wrought IN718 at room and elevated temperatures in long life regime. Specimens were undergone solution annealing at 940 °C for 2 h, air cooling, and then aging at 718 °C for 8 h, cooling to 621 °C with the rate of 50 °C/h and aging at this temperature for 8 h, followed by air cooling. They reported higher fatigue resistance in the high cycle regime at elevated temperatures as compared to the ones tested at room temperature. Fournier and Pineau [24] showed lower fatigue resistance in low cycle fatigue regime for wrought IN718 specimens at elevated temperature as compared to the specimens tested at room temperature. They discovered the fatigue fracture mechanism for wrought IN718 to be a mixture of transgranular and intergranular at elevated temperature, while it was observed to be transgranular at room temperature.

Considering the fact that IN718 is often used in applications prone to cyclic loading at elevated temperatures (e.g. turbine blades, jet engines, etc.), it is crucial to understand the fatigue behavior of AM IN718 at elevated temperatures for qualification and certification purposes [26]. In this paper, the fully-reversed, strain-controlled fatigue behavior of LB-DED IN718 is investigated at elevated temperature (650 °C), and the results are compared with those of the wrought specimens at elevated temperature as well as with the LB-DED IN718 fatigue tests at room temperature, both taken from literature. The fatigue performance of the material is discussed with the microstructural evolution during fatigue testing at elevated temperature. In addition, fracture mechanisms at elevated temperature are evaluated and compared to those from fatigue testing at room temperature. Finally, room and elevated temperature fatigue results of LB-DED IN718 specimens are compared with the ones of wrought counterparts taken from literature.

2. Experimental procedures

2.1. Material and specimen fabrication

The plasma rotating electrode processed (PREP) IN718 powder with the powder particle size in the range of 45–150 μm was utilized in this study. An OPTOMEC LENS™ 750, an LB-DED AM technique, was used to fabricate all the specimens. Argon gas was purged as the shielding gas during fabrication to protect the melt pool from the surrounded deleterious gases such as oxygen.

To determine the optimal values of the laser power, powder flow rate, and hatch spacing, a preliminary single-track study was conducted. As seen in Fig. 1(a), six single tracks were printed using different combinations of the aforementioned process parameters. Each deposited single track layer was cross sectioned (Fig. 1(b)), and characterized for the presence of defects (Fig. 1(c). Among the results obtained, the optimized process parameters were selected and listed in Table 1 [16].

Fig. 2 represents the cross direction raster scanning (CDRS) strategy [27] used in this study to fabricated specimens. The red color shows when the laser is on and the black color shows the previous location of the laser. As can be seen, this scanning strategy is comprised of contouring followed by printing the core of the specimen. It is worth noting that the laser rotates 90° for printing each subsequent layer.

Cylindrical rods with a diameter of 8 mm and length of 80 mm were fabricated. Fig. 3(a) shows the as-fabricated cylindrical specimen, which was further machined and polished into the fatigue specimens, for which the final geometry and dimensions are given in Fig. 3(b). It should be noted that the specimen diameter chosen in this study is smaller than the one recommended by ASTM E606; however, other dimensions were chosen within the recommended range to minimize the stress concentration effects at intersect of the gage and shoulder [28]. Fatigue specimens were polished to a mirror-like surface finish in the gage section before testing. Specimens were heat treated based on the Aerospace Material Specification (AMS) 5596C [17]. First, specimens were annealed at 940 °C for 2 h followed by air cooling. Then, the annealed specimens were aged at 718 °C for 8 h, cooled to 621 °C with the rate of 50 °C/h and kept at this temperature for 8 h followed by air cooling. Argon gas was utilized during all the heat treatment steps to avoid oxidation.

2.2. Microstructure characterization

In order to investigate the effect of heat treatment and fatigue testing at elevated temperature on the microstructural evolution, the microstructure of all conditions (i.e. as-built, heat treated, and cyclically deformed at elevated temperature) was characterized. The specimens were cut transversely parallel to the build direction, mounted and ground with sandpapers with grits ranging 320 (grain size of 46.3 μm)-4000 (grain size of 5 μm), followed by polishing to a mirror-like surface finish. The microstructure was further revealed using waterless Kalling's reagent, and a KEYENCE digital microscope as well as a Zeiss Crossbeam 550 scanning electron microscope (SEM) were used for the microstructural characterization.

2.3. Mechanical properties

For all the mechanical tests (i.e. tensile and uniaxial fully-reversed strain-controlled fatigue tests), an MTS landmark servo-hydraulic testing machine with a 100 kN load cell was employed. For measuring the strain meticulously, an MTS mechanical extensometer with the ceramic blades was attached to the specimens at the gage section during the test. Tensile tests were conducted at room temperature under 0.001 s^{-1} strain rate on the heat treated specimens. Two tensile tests were performed to assure the consistency of the results and the average is reported. Uniaxial fully-reversed strain-controlled fatigue tests were carried out at elevated temperature (650 °C).

For conducting high temperature fatigue tests, an MTS high temperature furnace at 650 °C and a high temperature MTS extensometer with ceramic blades were used. To only expose the gage section to the elevated temperature, the water cooling system was designed for the

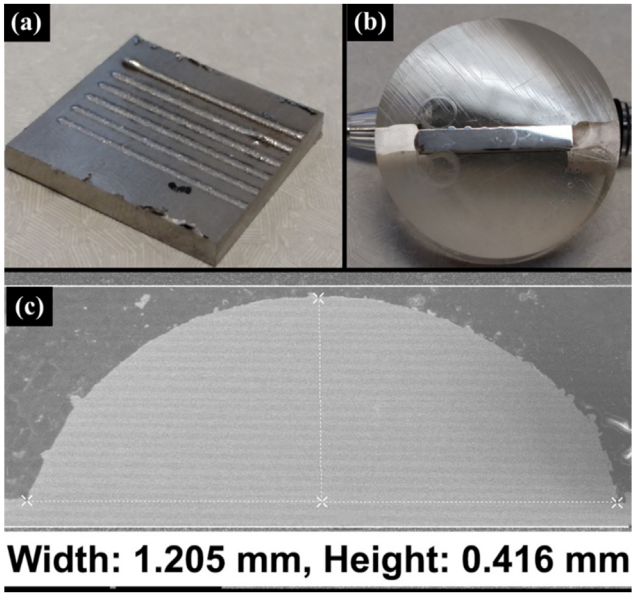

Fig. 1. A set of single-line deposition used to determine optimal process parameters for fabricating specimens with minimal defects: (a) six single tracks with different process parameters, (b) a cross-sectioned polished track, and (c) optical micrograph of the deposited material with the optimum process parameters.

Table 1
Optimized process parameters utilized in this study to fabricate LB-DED IN718 bars [16].

Laser power (W)	Scan speed (mm/s)	Powder flow rate (g/s)	Hatch spacing (mm)
350	15	0.057	0.529

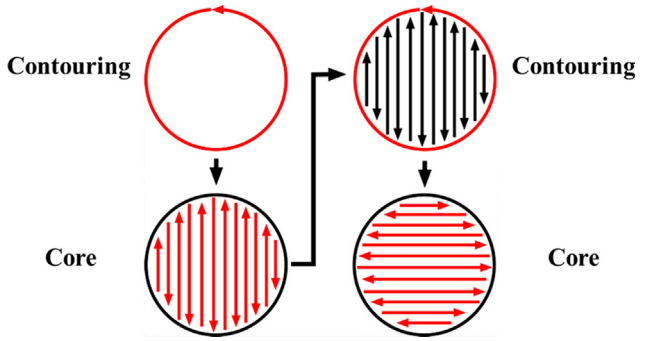

Fig. 2. The schematic of cross direction raster scanning strategy. The order of this scanning strategy is comprised of contouring + core + contouring. (Note: the red color is showing when the laser is on and printing, and the black color is showing the previous location of the laser). This image shows two consecutive layers. (For interpretation of the references to color in this figure legend, the reader is referred to the web version of this article.)

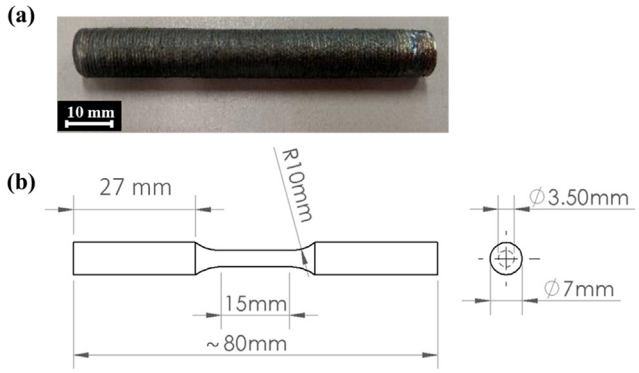

Fig. 3. (a) As-fabricated specimen, and (b) drawing showing the final geometry of specimens [29].

grips of the testing machine to keep the grip sections of the specimens cooled. It is worth noting that the gage section of specimens was kept at 650 °C for 30 min prior to start of fatigue testing to obtain a uniform temperature at the gage. Based on a recommendation by MTS for fatigue testing at elevated temperature using the extensometer with ceramic blades, the frequencies were adjusted to maximum 2 Hz for all the tests to avoid the extensometer slippage. The tests which continued over 10^6 reversals were considered as 'run-out' tests in this study.

In order to investigate the failure mechanisms at elevated temperature, fractography analysis was carried out on the fracture surfaces using SEM. Fracture surfaces were sonicated in water and alcohol solution first and then washed using acetone to clean any dirt or dust prior to fractography analysis.

3. Experimental results

3.1. Microstructure characterization and tensile behavior

The microstructure of LB-DED IN718 from the gage section of the as-built (i.e. non-heat treated) and heat treated specimens are presented in Fig. 4. As can be seen in Fig. 4(a), the as-built microstructure consists of columnar γ grains elongated parallel to the build direction as well as fine equiaxed grains adjacent to the fusion boundaries, shown with black dashed-lines. Moreover, the dendritic structure is seen inside the γ grains. The columnar grains as well as the dendritic structure are more obvious in the higher magnification micrograph presented.

Fig. 4(b) represents the microstructure of LB-DED IN718 after AMS 5596C heat treatment. As seen the dendritic structure was eliminated to some extent; however, they are still present in the fusion zones. There are also needle-like δ phases formed in the microstructure after the heat treatment, which are shown with red arrows. The needle-like δ phases in the microstructure formed after heat treatment are shown in the right side of Fig. 4(b) in higher magnification by red arrows.

The room temperature true stress-true strain curve as well as the strain hardening curve of LB-DED IN718 in heat treated condition are displayed in Fig. 5. It is worth noting that the strain hardening analysis was done beyond the yield strain (i.e. ε_y = 0.002 mm/mm). As seen in Fig. 5, the material exhibits a two-stage strain hardening behavior; stage I, an abrupt decrease in strain hardening, followed by stage II, a somewhat plateau in strain hardening behavior.

In addition, the detailed tensile properties are listed in Table 2, and the results are compared with those of the LB-DED IN718 fabricated with different powder conditions (i.e. PREP and gas atomized) as well as with those of the wrought IN718 [14,30]. Based on the results, although the experimental material in this study possesses lower yield strength as compared to the LB-DED IN718 fabricated with PREP/gas atomized powder and the wrought counterparts, it exhibits higher ultimate tensile strength (UTS) and elongation to failure. The latter was calculated based on the change in the final length of the deformed specimen relative to its initial length.

3.2. Fatigue behavior and properties

Fig. 6 shows the stable hysteresis loops of fully-reversed strain-controlled fatigue tests for LB-DED IN718 under various strain amplitudes tested at elevated temperature and room temperature [16]. As seen in Fig. 6(a), there is no plastic deformation at 0.002 mm/mm strain amplitude, neither for the fatigue test at room temperature nor for the one tested at elevated temperature. However, as the strain amplitude increases (Fig. 6(b) and (c)), LB-DED IN718 exhibits plastic deformation behavior in both testing temperature conditions. Fig. 6(b) represents hysteresis loops at 0.005 mm/mm strain amplitude showing slightly thinner hysteresis loop and lower extremum stresses for the test at 650 °C as compared to the one tested at room temperature. The latter may be attributed to the softening of γ matrix in the microstructure of the material during high temperature deformation. The thinner hysteresis loop is an indication of less plastic deformation occurring at the elevated temperature as compared to the room temperature testing condition.

At higher strain amplitude, 0.01 mm/mm, presented in Fig. 6(c), the material possesses more plastic deformation in both room and elevated temperature as compared to the lower strain amplitudes. In addition, similar to 0.005 mm/mm strain amplitude, the LB-DED IN718 tested at elevated temperature possesses less plastic deformation (i.e. thinner hysteresis loop) when compared to the one tested at room temperature.

The results of fully-reversed fatigue tests including strain amplitude, ε_a, elastic strain amplitude, $\frac{\Delta\varepsilon_e}{2}$, plastic strain amplitude, $\frac{\Delta\varepsilon_p}{2}$, mid-cycle stress amplitude, σ_a, mid-cycle mean stress, σ_m, and reversals to failure, $2N_f$, for LB-DED IN718 specimens tested at elevated temperature, are listed in Table 3. The values of the plastic strain amplitude were calculated by subtracting the elastic strain amplitude from the total strain amplitude. There are also some tensile/compressive mean stresses observed in these tests; however, in most cases, with exception of one test, the values are less than 10% of the stress amplitude, which should not have much influence on the fatigue behavior.

The Coffin-Manson relationship [31] considers the sum of elastic

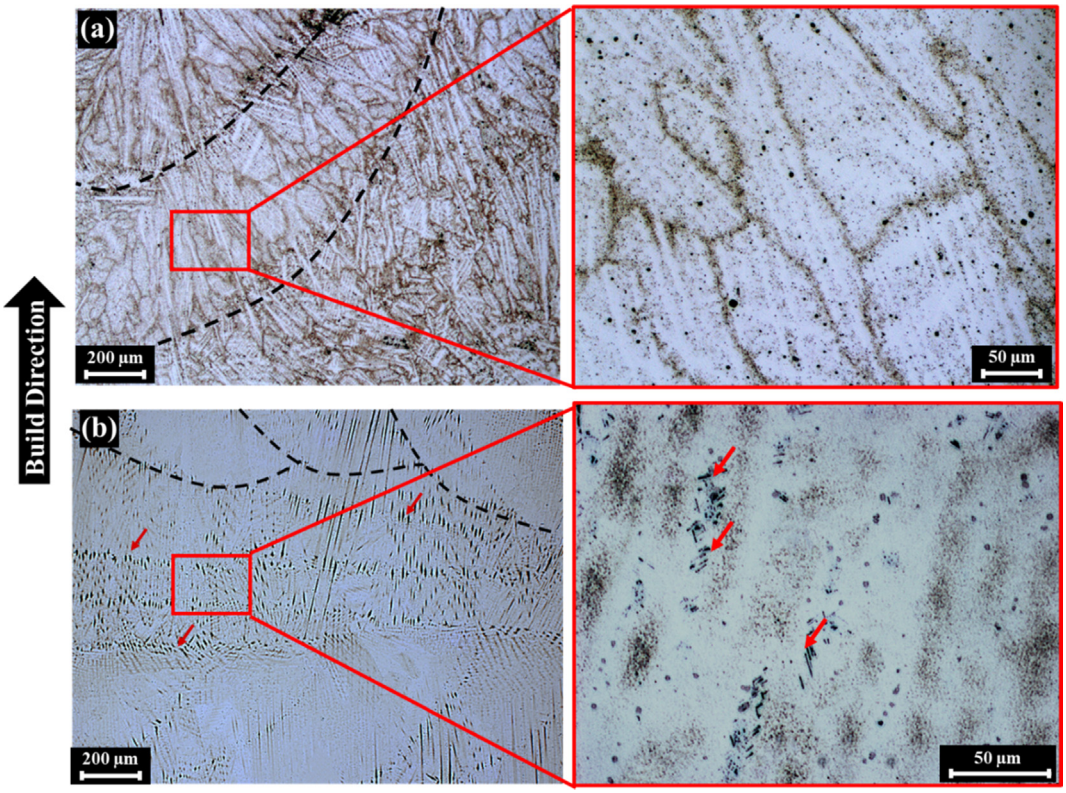

Fig. 4. Microstructures of LB-DED IN718 in (a) as-built, and (b) AMS 5596C heat treated conditions. The black dashed lines are showing the fusion zones and the red arrows are pointing the needle-like δ phases.

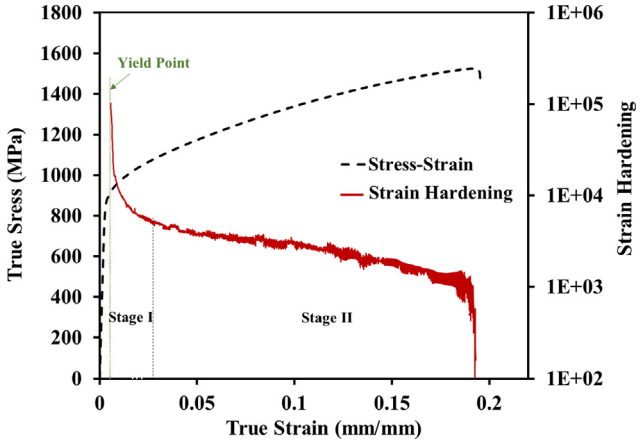

Fig. 5. Room temperature true stress-strain behavior of LB-DED IN718 in AMS 5596C heat treated condition along with the strain hardening curve embedded.

and plastic portions of strain to calculate the total strain amplitude:

$$\frac{\Delta\varepsilon}{2} = \varepsilon_a = \frac{\Delta\varepsilon_a}{2} + \frac{\Delta\varepsilon_p}{2} = \frac{\sigma_f^{'}}{E}(2N_f)^b + \varepsilon_f^{'}(2N_f)^c \quad (1)$$

where $\frac{\Delta\varepsilon_a}{2}$, $\frac{\Delta\varepsilon_p}{2}$, $\sigma_f^{'}$, E, $\varepsilon_f^{'}$, b, c, and $2N_f$ are elastic strain amplitude, plastic strain amplitude, fatigue strength coefficient, modulus of elasticity, fatigue ductility coefficient, fatigue strength exponent, fatigue ductility exponent, and reversals to failure, respectively. Fig. 7 shows the elastic, plastic, and total strain amplitude of LB-DED IN718 versus reversals to failure for tests conducted at elevated temperature. It can be seen that the total strain curve tends toward the plastic portion of the strain in high strain amplitude levels, while tents to elastic portion of the strain at low strain amplitude levels. The fatigue properties obtained at room temperature [16] and elevated temperatures are listed in Table 4. It is worth mentioning that the run-out results were excluded to get the best fit.

Fig. 8 shows the comparison of strain-life fatigue behavior of LB-DED IN718 specimens tested at room temperature and elevated temperature [29]. As observed in low cycle fatigue regime (i.e. high strain amplitude level), the LB-DED IN718 material tested at room temperature possesses slightly higher fatigue resistance (i.e. longer fatigue lives) than those tested at elevated temperature. However, the fatigue lives

Table 2
Monotonic room temperature tensile properties of LB-DED IN718 in heat treated condition from this study as well as LB-DED IN718 and wrought counterparts adopted from [30] and [14].

Material	Solution annealed temperature	YS (MPa)	UTS (MPa)	EL (%)
Heat treated LB-DED IN718 (this study and PREP powder)	940 °C	895 ± 38	1514 ± 21	19.7 ± 0.45
Heat treated LB-DED IN718 [14]	980 °C	1257	1436	13
Heat treated LB-DED IN718 (PREP powder) [30]	1080 °C + 980 °C	1170	1360	18
Heat treated LB-DED IN718 (gas atomized powder) [30]	1080 °C + 980 °C	1133	1240	9
Heat treated Wrought IN718 [30]	1080 °C + 980 °C	1100	1340	12
Heat treated Wrought IN718 [14]	980 °C	1125	1365	20

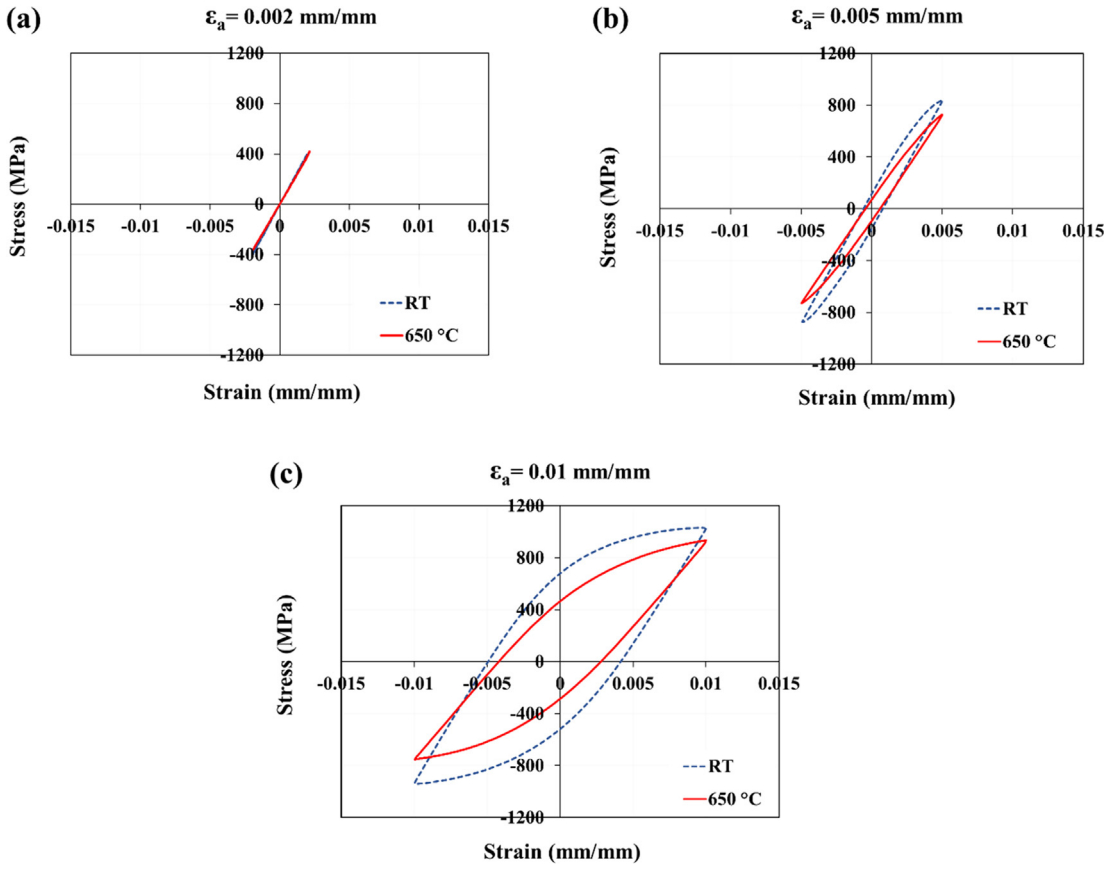

Fig. 6. Stable hysteresis loops of fully-reversed strain-controlled constant amplitude fatigue tests of LB-DED IN718 at elevated temperature as well as room temperature [16] at different strain amplitudes: (a) 0.002 mm/mm, (b) 0.005 mm/mm, and (c) 0.01 mm/mm.

Table 3
Uniaxial fully-reversed fatigue test results for LB-DED IN718 specimens at elevated temperatures.

ε_a (mm/mm)	$\frac{\Delta\varepsilon_e}{2}$ (mm/mm)	$\frac{\Delta\varepsilon_p}{2}$ (mm/mm)	σ_a (MPa)	σ_m (MPa)	$2N_f$ (Reversals)
0.0013	0.0013	0	230	1	> 20,003,884
0.0020	0.0020	0	413	22	> 10,638,354
0.0030	0.0030	0	588	22	127,436
0.0038	0.0030	0.0008	637	6	140,766
0.0040	0.0038	0.0002	635	26	22,688
0.0050	0.0043	0.0007	731	−10	13,430
0.0050	0.0040	0.0010	733	2	12,420
0.0060	0.0044	0.0016	795	−5	3,154
0.0063	0.0047	0.0016	858	103	4,446
0.0075	0.0042	0.0033	830	−8	1,838
0.0080	0.0052	0.0028	842	34	1,774
0.0100	0.0061	0.0039	854	88	894
0.0100	0.0047	0.0053	963	14	396

become much more similar as the strain amplitude decreases. Eventually, it can be noticed that the material exhibits very similar fatigue behavior regardless of testing temperature in the high cycle fatigue regime (i.e. strain amplitudes less than 0.005 mm/mm). Interestingly, it has been reported that in the high cycle fatigue regime the wrought IN718 possesses a higher fatigue strength at elevated temperature than the room temperature due to the γ-matrix softening and surface oxidation occurring at elevated temperature [23].

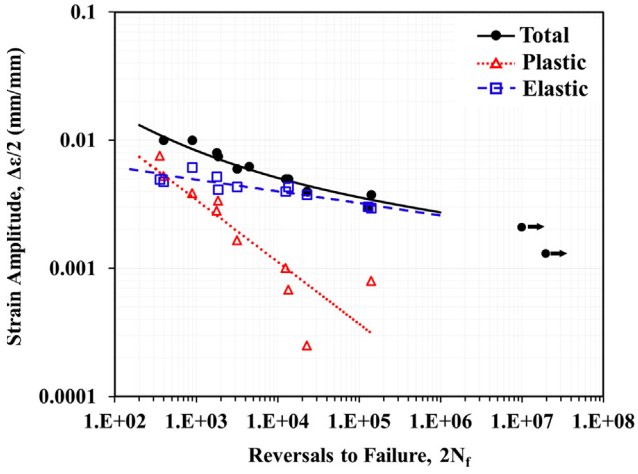

Fig. 7. Total, elastic, and plastic strain amplitudes versus reversals to failure for fully-reversed, strain-controlled fatigue tests of LB-DED IN718 specimens at elevated temperature (i.e. 650 °C).

Table 4
Fatigue properties of LB-DED IN718 at room [16] and elevated temperatures.

Test condition	σ_f' (MPa)	b	ε_f' (mm/mm)	c
RT [16]	2090	−0.111	1.8	−0.78
650 °C	1708	−0.092	0.1	−0.48

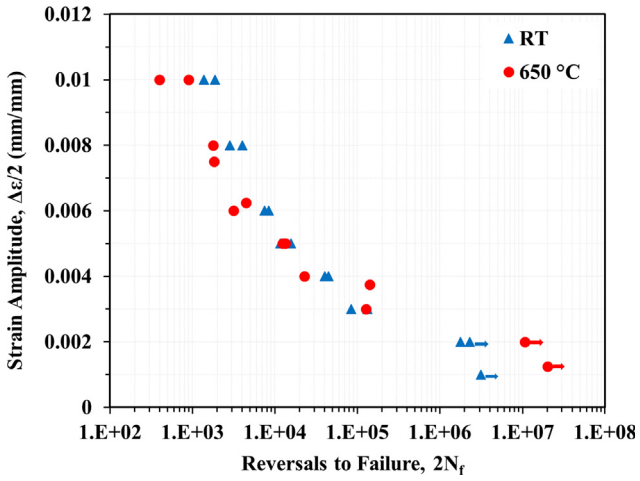

Fig. 8. The comparison of strain-life fatigue behaviors of LB-DED IN718 specimens at room temperature [16] and elevated temperature.

4. Discussion on experimental observations

4.1. Tensile behavior

Fig. 5 shows the room temperature true stress-true strain curve as well as the strain hardening curve of heat treated LB-DED IN718 generated in this study. It can be seen from the stress-strain curve (black dashed-line in Fig. 5) that the material strain hardens gradually after the onset of plastic deformation (i.e. beyond the yield strain). Looking at the strain hardening curve, it includes two stages; stage I for the strain hardening behavior right after onset of plastic deformation (i.e. yielding) and stage II for the strain hardening response of material by increasing the strain until fracture. The abrupt drop in the strain hardening in stage I is attributed to the dislocation gliding mechanism in the early stage of plastic deformation after yielding [32]. However, this reduction of strain hardening slows down by increasing the applied strain at stage II.

Due to the low temperature solution heat treatment procedure performed in this study (940 °C) as compared to the temperature required for complete solution of the γ′ and γ″ precipitates (i.e. 1060 °C [33]), γ′ and γ″ precipitates could not be resolved completely. Thus, the γ′ and γ″ precipitates may have been partially decomposed to the δ and Laves phases. The presence of these phases in the microstructure and their interaction with dislocations can result in the strain hardening of the material, as evident in Fig. 5.

It can be noted from Table 2 that the LB-DED IN718 material utilized in this study, while having higher ultimate tensile strength (UTS) and ductility, it possesses lower yield strength (YS) as compared to LB-DED IN718 data generated elsewhere [14,30]. This may be attributed to the variations of the precipitates in the microstructure of LB-DED IN718 specimens investigated here as compared to the other studies, which could have been caused by different heat treatment procedures utilized. It has been shown for the wrought IN718 that presence of δ phase in the microstructure decreases the YS and increases the UTS [33].

As compared to the tensile properties of the wrought IN718 [14,30] listed in Table 2, the LB-DED IN718 in the current study still exhibits a higher UTS. This again confirms the role of the solution annealing temperature on the formation of δ phase, which consequently affects the mechanical properties of IN718 [34]. In both studies by Blackwell [14] and Zhao et al. [30], the solution heat treatment temperatures utilized were higher than the one performed in this study. Therefore, lower δ phase in the microstructure of wrought IN718 [14,30] resulted in a higher YS and a lower UTS as compared to the LB-DED IN718 produced in this study.

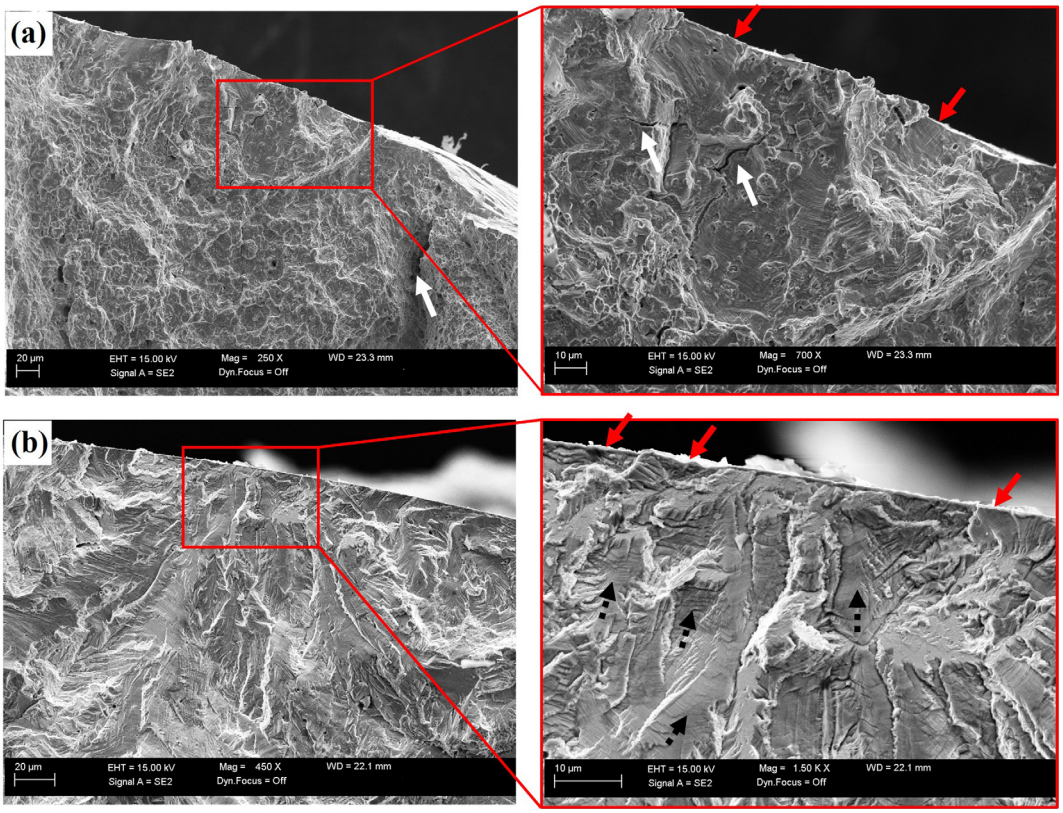

Fig. 9. Fracture surfaces of fatigue tests at elevated temperature (i.e. 650 °C): (a) 0.01 mm/mm strain amplitude, and (b) 0.003 mm/mm strain amplitude indicating the crack in both specimens originated from the surface shown by red arrows. Black dashed arrows indicate striations, and secondary cracks are shown with white arrows. (For interpretation of the references to color in this figure legend, the reader is referred to the web version of this article.)

4.2. Fatigue behavior

The fracture mechanism of the present LB-DED IN718 material at room temperature has been investigated by Johnson et al. in [16]. All the specimens tested at room temperature had a distinct crack growth region comprised of striation marks perpendicular to the crack growth path as well as the final fracture region with dimples representative of ductile fracture. The cracks have been found to be initiated from hard particles and/or pores close to the surface and propagated in transgranular mode all the way up to the final fracture stage.

Fracture surfaces of two LB-DED IN718 specimens tested in this study at the elevated temperature at two different strain amplitudes of 0.01 mm/mm and 0.003 mm/mm are presented in Fig. 9(a) and (b), respectively. In both strain amplitude levels, cracks initiated from the surface shown by red arrows. It can be seen in Fig. 9(a) that there is sufficient fraction of areas showing tortuous features (bright white areas) for the specimen tested at 0.01 mm/mm strain amplitude, while the fracture surface of the specimen tested at 0.003 mm/mm strain amplitude (Fig. 9(b)) is mostly constituent of smooth cleaved facets.

There are secondary cracks observed on the fracture surface of specimen tested at 0.01 mm/mm strain amplitude, shown by white arrows in Fig. 9(a). These secondary cracks were observed mostly on the fracture surface of specimens tested at higher strain amplitude levels. This may be ascribed to the presence of brittle δ and Laves phases on the grain boundaries that can break under larger deformation and create the secondary cracks. Based on the features seen on the fracture surfaces (i.e. secondary cracks) for the specimens at higher strain amplitude levels (i.e. low cycle fatigue regime) tested at elevated temperature, the crack growth mode is intergranular and different than the transgranular crack growth observed for LB-DED IN718 specimens tested at room temperature [16].

At lower strain amplitude of 0.003 mm/mm (i.e. high cycle fatigue regime), the fracture surface shown in Fig. 9(b) is constituent of smooth cleaved facets and striation marks (shown by black dashed-arrows) representative of a transgranular fracture. In fact, the deformation applied in the high cycle fatigue regime may not be sufficiently high to break the δ and Laves phases on the grain boundaries. It has been reported that the δ and Laves phases in the microstructure of LB-DED IN718 maintain their morphologies at low stress amplitudes (i.e. high cycle fatigue regime), and short cracks have to detour these phases and propagate in the γ matrix [21].

As was presented in Fig. 8, the LB-DED IN718 possesses somewhat similar fatigue performance at room temperature and elevated temperature. However, LB-DED IN718 tested at room temperature slightly outperformed the ones tested at elevated temperature in the low cycle fatigue regime. As it is well established, a considerable fraction of fatigue life in the low cycle fatigue regime is typically allocated to the crack growth stage [31]; therefore, the microstructural features should further affect the fatigue behavior in this life regime. Fig. 10 presents the microstructure of two LB-DED IN718 specimens after fatigue testing taken using SEM with back scattered detector (BSD); one at 0.01 mm/mm (Fig. 10(a)) and the other one at 0.004 mm/mm (Fig. 4(b)) strain amplitude at elevated temperature.

Comparing Figs. 10 and 4(b), considerable amount of fine needle-like δ phases and Laves phases, shown respectively by red and yellow dashed-arrows, are formed on the grain boundaries under cyclic loading at elevated temperature. In addition, comparing the microstructure of the specimen tested in low cycle fatigue regime (Fig. 10(a)) with that of the specimen tested in high cycle fatigue regime (Fig. 10(b)), higher fraction of δ phases and Laves phases were formed in the microstructure of the specimen tested at high cycle fatigue regime. This is due to the longer exposure to elevated temperature for specimens tested in the high cycle fatigue regime.

Carpenter et al. [35] reported the decomposition of γ″ to δ phase on the grain boundary of wrought IN718 due to the relatively low solution heat treatment temperature (982 °C). The selected heat treatment procedure may also cause the segregation of Nb in the grain boundaries which can lead into to the formation of Laves phases. The presence of δ and Laves phases was found to be the reason for the embrittlement of the grain boundaries providing an easy crack growth path in wrought IN718. It has been also shown for the LB-DED IN718 that at higher stress amplitude levels, the δ and Laves phases break apart and accelerate the fatigue damage in the material [21]. Accordingly, the secondary cracks observed on the fracture surfaces of the specimen tested at 0.01 mm/mm strain amplitude in Fig. 9(a), may represent the breakage of δ and Laves phases at the high strain amplitude, which have assisted with the fatigue damage in the material. In addition, the formation of more brittle δ and Laves phases (compare Fig. 10(a) with Fig. 4(b)), by exposing the specimen to elevated temperature, which includes keeping the specimen for 30 min at 650 °C followed by fatigue testing at 650 °C, can be responsible for somewhat shorter fatigue lives as compared to the LB-DED IN718 specimens tested at room temperature in the low cycle regime.

In the high cycle fatigue regime, however, the LB-DED IN718 possesses more or less similar fatigue behavior at room and elevated temperatures. On the contrary to the low cycle fatigue regime, a bigger portion of the fatigue life in the high cycle regime is typically spent in the crack initiation stage [31]. It has been reported for the wrought IN718 that formation of oxide films on the surface of specimens during fatigue testing at elevated temperature suppresses crack initiation caused by surface slipping (i.e. formation of intrusions and extrusions) [23]. These oxide films assisted with the closure of microstructurally short cracks and delayed the formation of macro cracks, thereby, increased the fatigue resistance.

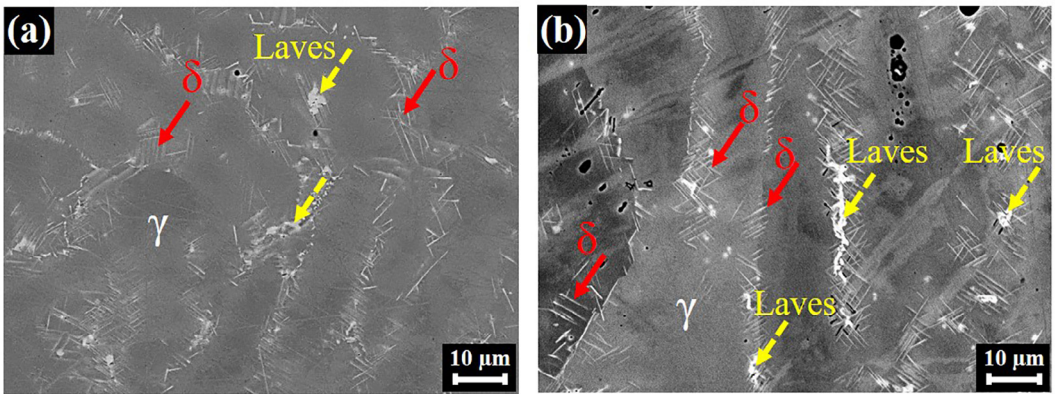

Fig. 10. The BSD images showing the microstructure of LB-DED IN718 after fatigue testing at elevated temperature at (a) 0.01 mm/mm strain amplitude, and (b) 0.004 mm/mm strain amplitude. The images present the γ matrix including the needle-like δ phases along with the Laves phases shown by red arrows and yellow dashed arrows, respectively. (For interpretation of the references to color in this figure legend, the reader is referred to the web version of this article.)

As it is observed in Fig. 9(b), the cracks initiated from the surface of the LB-DED IN718 specimens tested at elevated temperature. Therefore, similar to the crack initiation mechanism seen in wrought IN718 [23], the formation of oxide layers on the surface of LB-DED IN718 specimens tested at elevated temperature in the high cycle fatigue regime may be one of the reasons for their comparable fatigue lives with the specimens tested at room temperature. Although the δ and Laves phases are also capable of stopping and deflecting micro-cracks in the high cycle fatigue regime (i.e. low strain amplitude) [21], the higher fraction of these brittle phases formed during the longer fatigue testing at elevated temperature in the high cycle regime (see Fig. 10(b)) can be detrimental to the fatigue resistance of the material.

One reason for the comparable fatigue performance obtained for the LB-DED IN718 specimens tested at elevated temperature with room temperature in the high cycle regime, while for the wrought LB-PBF IN718 performed better at the elevated temperature than the room temperature, may be related to the different fatigue testing conducted for wrought specimen in [23], which was rotating fatigue testing as compared to the uniaxial fatigue testing in this study. Due to the stress gradient in the rotating bending fatigue testing, the maximum stress is applied only on the surface of the specimen; therefore, the oxide films may have more effects in closing micro-cracks and extending the fatigue life. However, the entire cross-sectional area in the uniaxial fatigue testing experiences the maximum stress and the effect of surface oxidation may not be as significant on the fatigue behavior. Additionally, some variations in the chemical composition of IN718 can affect its fatigue performance. For example, addition of an extra amount of Boron to IN718 results in higher fatigue crack growth resistance at elevated temperature than room temperature [36]. Moreover, alloying elements such as Ti, Cr, Co, and Mo in the chemical composition of nickel-base superalloys can alter the antiphase boundary energies and modify the reversibility of dislocation motion, which may affect the high cycle fatigue resistance of the material [37].

Fig. 11 compares the fatigue performance of LB-DED IN718 machined specimens with that of the wrought specimens both in room temperature and 650 °C (i.e. elevated temperature). The room temperature fatigue data for LB-DED IN718 material are adopted from [16], and the fatigue data for the wrought material in both room temperature and high temperature conditions are adopted from [17]. It must be noted that the heat treatment utilized herein and in [16] for the LB-DED IN718 is similar to the heat treatment procedure applied on the wrought specimens [17]. As can be seen in Fig. 11(a), the LB-DED IN718 possesses slightly lower fatigue resistance at room temperature as compared to the wrought counterpart, both in the low cycle and high cycle fatigue regimes. Interestingly, while wrought IN718 performs slightly better in the high cycle regime, the overall fatigue behavior of LB-DED IN718 at elevated temperature is somewhat similar to that of the wrought counterpart, as seen in Fig. 11(b).

Johnson et al. [16] attributed the lower fatigue resistance of LB-DED IN718 at room temperature compared to the wrought IN718 to the heterogeneous microstructure as well as the presence of defects (i.e. gas entrapped pores, or inclusions) in the LB-DED specimens. On the contrary, according to the Fig. 9 for the LB-DED IN718 specimens tested at elevated temperature, the cracks initiated from the surface. This means that the defects (gas entrapped pores, or inclusions) did not affect the fatigue behavior of LB-DED IN718 specimens at elevated temperature; therefore, the fatigue resistance of LB-DED IN718 is similar to that of the wrought material (Fig. 11(b)).

5. Conclusions

Fatigue behavior of LB-DED IN718 at elevated temperature (650 °C) was investigated and compared to that of LB-DED IN718 at room temperature as well as the wrought counterparts at room and elevated temperatures. The microstructural evolution and fracture mechanisms were also characterized. The major conclusions based on the experimental results and discussions can be listed as:

1. LB-DED IN718 specimens undergone AMS 5596C heat treatment exhibited lower room temperature YS and higher UTS as compared to the wrought and LB-DED counterparts which have been solution heat treated at higher temperatures. This may be attributed to the presence of δ and Laves phases formed as a result of partial decomposition of γ′ and γ″ precipitates due to the lower temperature solution heat treatment performed in this study.
2. Fractography analysis of the LB-DED IN718 cyclically deformed at elevate temperature revealed intergranular fatigue crack growth mode in low cycle fatigue regime, and transgranular crack growth mode in high cycle fatigue regime.
3. LB-DED IN718 had an inferior low cycle fatigue resistance at elevated temperature than room temperature. This may be due to the formation of more δ and Laves phases during fatigue testing at elevated temperature. These brittle phases can break under high strains and accelerate the fatigue damage by providing an easier crack growth path.
4. Comparable high cycle fatigue lives were obtained for LB-DED IN718 specimens tested at elevated and room temperatures. This was attributed to the surface oxidation during fatigue testing at elevated temperature, which could suppress crack initiation and assist with the closure of microstructurally short cracks.
5. Elevated temperature fatigue resistance of LB-DED IN718 was found to be similar to that of the wrought counterpart. Fractography analysis of LB-DED specimens revealed all the cracks to initiate from

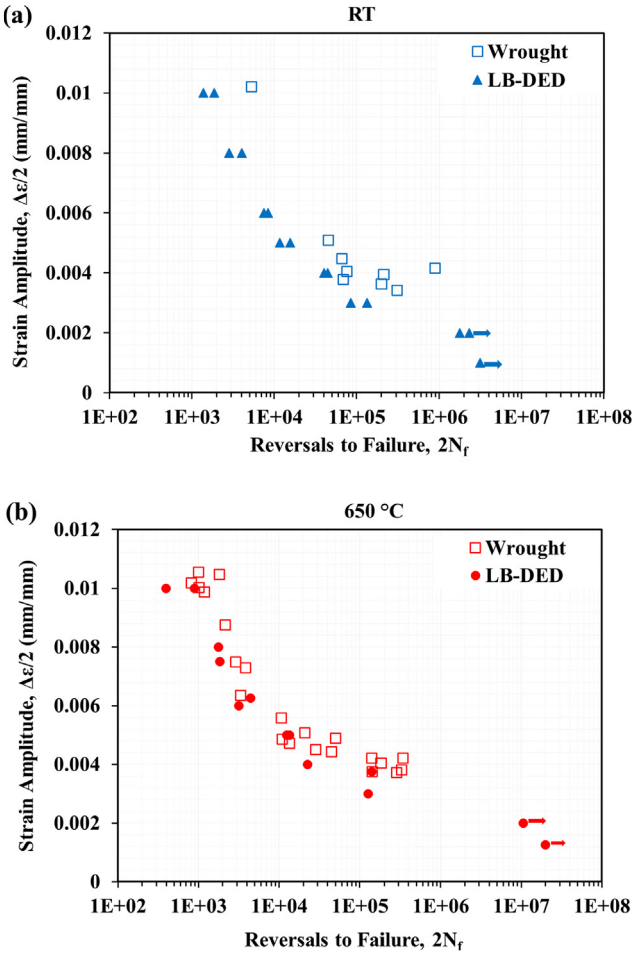

Fig. 11. Comparison of strain-life fatigue data of LB-DED and wrought IN718 at (a) room temperature (LB-DED data adopted from [16]), and (b) elevated temperature (650 °C). All the wrought data are adopted from [17]

the surface at elevated temperature fatigue testing, indicating no effect of defects (i.e. pores, lack of fusion) on the fatigue behavior.

Declaration of Competing Interest

The authors declare that they have no known competing financial interests or personal relationships that could have appeared to influence the work reported in this paper.

Acknowledgments

Most of the experiments for this study were conducted while ASJ was performing his graduate research at Mississippi State University under the direction of NS.

References

[1] Akca E, Gursel A. A review on superalloys and IN718 Nickel-based Inconel superalloy. Period Eng Nat Sci 2015;3.
[2] Keiser DD, Brown HL. A review of the physical metallurgy of alloy 718; 1976.
[3] Nunes RM, Pereira D, Clarke T, Hirsch TK. Delta phase characterization in Inconel 718 alloys through x-ray diffraction. ISIJ Int 2015;55:2450–4.
[4] Kumara C, Segerstark A, Hanning F, Dixit N, Joshi S, Moverare J, et al. Microstructure modelling of laser metal powder directed energy deposition of alloy 718. Addit Manuf 2019;25:357–64.
[5] Thakur DG, Ramamoorthy B, Vijayaraghavan L. Machinability investigation of Inconel 718 in high-speed turning. Int J Adv Manuf Technol 2009;45:421–9.
[6] Shamsaei N, Yadollahi A, Bian L, Thompson SM. An overview of Direct Laser Deposition for additive manufacturing; Part II: mechanical behavior, process parameter optimization and control. Addit Manuf 2015;8:12–35.
[7] Masoomi M, Pegues JW, Thompson SM, Shamsaei N. A numerical and experimental investigation of convective heat transfer during laser-powder bed fusion. Addit Manuf 2018;22:729–45.
[8] Seifi M, Gorelik M, Waller J, Hrabe N, Shamsaei N, Daniewicz S, et al. Progress towards metal additive manufacturing standardization to support qualification and certification. JOM 2017;69:439–55.
[9] Carroll BE, Palmer TA, Beese AM. Anisotropic tensile behavior of Ti–6Al–4V components fabricated with directed energy deposition additive manufacturing. Acta Mater 2015;87:309–20.
[10] Wang Z, Palmer TA, Beese AM. Effect of processing parameters on microstructure and tensile properties of austenitic stainless steel 304L made by directed energy deposition additive manufacturing. Acta Mater 2016;110:226–35.
[11] Alnajjar M, Christien F, Wolski K, Bosch C. Evidence of austenite by-passing in a stainless steel obtained from laser melting additive manufacturing. Addit Manuf 2019;25:187–95.
[12] Yadollahi A, Shamsaei N, Thompson SM, Elwany A, Bian L. Effects of building orientation and heat treatment on fatigue behavior of selective laser melted 17–4 PH stainless steel. Int J Fatigue 2017;94:218–35.
[13] Lambarri J, Leunda J, García Navas V, Soriano C, Sanz C. Microstructural and tensile characterization of Inconel 718 laser coatings for aeronautic components. Opt Lasers Eng 2013;51:813–21.
[14] Blackwell PL. The mechanical and microstructural characteristics of laser-deposited IN718. J Mater Process Technol 2005;170:240–6.
[15] Zhai Y, Lados DA, Brown EJ, Vigilante GN. Understanding the microstructure and mechanical properties of Ti-6Al-4V and Inconel 718 alloys manufactured by Laser Engineered Net Shaping. Addit Manuf 2019;27:334–44.
[16] Johnson AS, Shao S, Shamsaei N, Thompson SM, Bian L. Microstructure, fatigue behavior, and failure mechanisms of direct laser-deposited Inconel 718. JOM 2016;69.
[17] Brinkman CR, Korth GE. Strain fatigue and tensile behavior of Inconel 718 from room temperature to 650°C. J Test Eval 1974.
[18] Komarasamy M, Shukla S, Williams S, Kandasamy K, Kelly S, Mishra RS. Microstructure, fatigue, and impact toughness properties of additively manufactured nickel alloy 718. Addit Manuf 2019;28:661–75.
[19] Wan HY, Zhou ZJ, Li CP, Chen GF, Zhang GP. Enhancing fatigue strength of selective laser melting-fabricated Inconel 718 by tailoring heat treatment route. Adv Eng Mater 2018;20:1800307.
[20] Balachandramurthi AR, Moverare J, Dixit N, Deng D, Pederson R. Microstructural influence on fatigue crack propagation during high cycle fatigue testing of additively manufactured Alloy 718. Mater Charact 2019;149:82–94.
[21] Sui S, Chen J, Fan E, Yang H, Lin X, Huang W. The influence of Laves phases on the high-cycle fatigue behavior of laser additive manufactured Inconel 718. Mater Sci Eng A 2017;695:6–13.
[22] Yan N, Kawagoishi N, Chen Q, Wang QY, Nisitani H, Kondo E. Fatigue properties of Inconel 718 in long life region at elevated temperature; 2003.
[23] Kawagoishi N, Chen Q, Nisitani H. Fatigue strength of Inconel 718 at elevated temperatures. Fatigue Fract Eng Mater Struct 2000;23:209–16.
[24] Fournier D, Pineau A. Low cycle fatigue behavior of Inconel 718 at 298 K and 823 K. Metall Trans A 1977;8:1095–105.
[25] Chen Q, Kawagoishi N, Nisitani H. Evaluation of notched fatigue strength at elevated temperature by linear notch mechanics. Int J Fatigue 1999;21:925–31.
[26] Russell R, Wells D, Waller J, Poorganji B, Ott E, Nakagawa T, Sandoval H, Shamsaei N, Seifi M. Qualification and certification of metal additive manufactured hardware for aerospace applications. Addit Manuf Aerosp Ind 2019:33–66.
[27] Jinoop A, Paul C, Bindra K. Laser-assisted directed energy deposition of nickel super alloys: a review. Proc Inst Mech Eng Part L J Mater Des Appl 2019. 146442071985265.
[28] ASTM E606. − 12, Standard test method for strain-controlled fatigue testing, ASTM Int.; 2012.
[29] Johnson AS, Shrestha R, Nezhadfar PD, Shamsaei N. Fatigue behavior of laser beam directed energy deposited Inconel 718 at elevated temperature. Proceedings of the 30th annual international solid freeform fabrication symposium – an additive manufacturing conference. 2019.
[30] Zhao X, Chen J, Lin X, Huang W. Study on microstructure and mechanical properties of laser rapid forming Inconel 718. Mater Sci Eng A 2008;478:119–24.
[31] Stephens RI, Fatemi A, Stephens RR, Fuchs HO. Metal fatigue in engineering. John Wiley & Sons; 2000.
[32] Dieter GE, Bacon DJ. Mechanical metallurgy. New York: McGraw-hill; 1986.
[33] Moiz M. The influence of grain size on the mechanical properties of Inconel 718; 2013.
[34] Tucho WM, Cuvillier P, Sjolyst-Kverneland A, Hansen V. Microstructure and hardness studies of Inconel 718 manufactured by selective laser melting before and after solution heat treatment. Mater Sci Eng A 2017;689:220–32.
[35] Carpenter W, Kang S-J, Chang KM. SAGBO mechanism on high temperature cracking behavior of Ni-base superalloys; 1997.
[36] Xiao L, Chen DL, Chaturvedi MC. Effect of boron on fatigue crack growth behavior in superalloy IN 718 at RT and 650 °C. Mater Sci and Eng A 2016;428:1–11.
[37] Dodaran M, Ettefagh AH, Guo SM, Khonsari MM, Meng WJ, Shamsaei N, et al. Effect of alloying elements on the γ' antiphase boundary energy in Ni-base superalloys. Intermetallics 2020;117.